THERMAL PERFORMANCE CHARACTERISATION OF A NOVEL HYBRID FIBRE REINFORCED TIMBER (HFT) COMPOSITE WALL SYSTEM USING THE TRANSIENT DATA ASSIMILATION (TDA) METHOD

G. Soret[1]*, Hao Zhou[1], J. Hidalgo[1], J. Carrascal[1], J.L. Torero[2], D. Fernando[1]

ABSTRACT: Building envelope thermal performance requirements are becoming stricter to support the government commitments to reduce greenhouse gas emissions (GHG). To effectively achieve such obligations, current standard methods used by designers to characterize insulating properties like the thermal resistance (R-value) may not be enough. This study demonstrated such approach by comparing the overall R-value of a novel Hybrid Fibre reinforced Timber (HFT) composite wall system calculated using standard analytical methods and the Transient Data Assimilation (TDA) method. During the process, it was evaluated the contribution of the HFT elements and air cavities to its overall R-value. This study showed that the air cavities of a timber made building envelope component may conduct more heat than the structural elements, despite that it is generally accepted that they contribute positively to the overall R-value. Further, this study revealed that the insulating properties of air cavities calculated by means of standard analytical methods may underestimate the Heating, Ventilation, and Air Conditioning (HVAC) loads needed to keep comfort conditions in a building, resulting in an unexpected increased use of energy and associated GHG. These are findings that not only influence the HFT design decision process but also suggest revisiting existing standard methods.

KEYWORDS: timber, R-value, thermal insulation, thermal bridge, air cavity.

1 – INTRODUCTION

The world is becoming warmer, and as a result, the electricity demand to keep building comfort conditions by means of building cooling systems is increasing. The thermal performance of building envelopes will have a visible impact on such a demand, together with the associated increase greenhouse emissions and household electricity bills [1]. In this regard, the steady-state thermal resistance, the R-value, is the most representative parameter that describe the insulating capabilities of building components [2]. Regarding to this, the most accurate method to determine the overall R-value of a building envelope system is by means of conducting a test, such as the Guarded Hot Box standard apparatus [3, 4], which generally incurs high costs [5].

Although there have been many versions of the Hot Box apparatus, the fundamental principles of the Hot Box apparatus remain the same since its first conception in 1912 by the National Institute of Standards and Technology (NIST). Representative examples are the small hot box developed by Peters et al [6], the modified Guarded Hot Box apparatus used by Kamil et al [7], and more recently the use of the Hot Box to measure the thermal resistance of multilayer reflective insulation products [8].

All the Hot Box versions considered measurements conducted only at the exterior of the building envelope system. Current climate change challenges require more detailed description of heat transfer processes in the building envelope systems so that a more building energy efficient designs can be achieved. This approach is assisted by the use of thermal test methods as reliable as the hot box measurements however including measurements in the interior of the building envelope components such as the TDA method developed by Soret et al [9].

This study focused on understanding the internal heat flow processes happening on a novel HFT wall system

[1] School of Civil Engineering, Building 49 Advanced Engineering Building, Staff House Road, The University of Queensland, St Lucia, QLD 4072, Australia

[2] Department of Civil, Environmental & Geomatic Engineering, University College London, UK

https://doi.org/10.52202/080513-0099

affecting its overall R-value to evaluate further changes on either the geometry or the materials considered to achieve the design objectives. In this regard, the project pursued evaluating the effect of the structural elements and the effect of the air cavities on the overall R-value of the system.

1.2 THERMAL BRIDGES IN THE BUILDING ENVELOPE.

Building envelopes have multiple functions that influence each other and therefore need to be considered in a holistic manner. This is the case of primary functions such as reducing the energy consumption to keep internal building comfort conditions and, indeed, providing the building envelope with the ability to support both internal and external forces and achieve structural integrity [10]. Often, the building elements used to achieve the latter, include thermal properties that are detrimental for the former. This is the case of structural elements made of metallic materials that naturally comes with high thermal conductivities which facilitates the pass of the heat from the exterior to the interior of the building and vice versa, acting as a form of "thermal bridges". Such approach can be observed for example in curtain and metal stud-wall constructions [5], and even on building envelopes made of Cross Laminated Timber (CLT) due to the necessary structural connections required [11].

1.3 THE THERMAL PERFORMANCE OF AIR CAVITIES

Heat pass through the air by radiation and convection heat transfer processes. The internal features of a building system cannot be validated against the Hot Box data since only external data is measured. Thus, aspects such the contribution of an air cavity to the overall R-value of a building system cannot be measured specifically. Nevertheless, methods such as the TDA does allow a direct measurement of each layer of a building system, in particular, the measurement of the equivalent thermal conductivity for air cavities.

The thermal resistance of an air cavity of a building system change depending on the surface of the system that is exposed to heat (such as external cladding or internal lining in a building wall system) due to the changes of the thermal conditions in the cavity that change on the direction of the heat flow. This can be easily understood by observing the temperature distribution through a system in both cases. Indeed, the influence of the thermal resistance of the air cavity may influence the overall thermal resistance of the building system. This was observed by Soret et al [9] on an Light steel frame (LSF) system where the system Rc;op (i.e., the surface-to-surface R-value) varied approx. 25% when the heat load was applied to both the external cladding and the internal lining.

2 – BACKGROUND

This study focussed on a novel hybrid fibre reinforced timber (HFT) composite wall system wall system developed by Fernando et al in a research project [12, 13] that explores design methods to achieve both structural and thermal performance optimisation of a building along with other important architectural aspects such buildability and cost-efficiency.

3 – PROJECT DESCRIPTION

Soret et al [9] developed the TDA method to obtain the R-value of building envelop systems and demonstrated to be as accurate as those using the standardized Hot Box apparatus. The TDA method appeared to also be simpler and, importantly, provide detailed information of the internal hat flow processes happening in the building component. Therefore, this method fitted well in the overall research approach.

4 – EXPERIMENTAL SETUP

The TDA method consisted of a small-scale thermal test combined with a numerical thermal model of the HFT composite system sampled. The thermal test was used to monitor the sample both internally and externally. A stainless steel 5 kW electric radiant heater with a rectangular shape and two bulbs (Infratech WD 5024 Series) was used to apply a heat load on one surface of the building system from ambient temperature until steady heat flow conditions within the system were attained. A heat flux meter was used (SBG01 Hukseflux) to measure the heater heat load capability. In-depth thermal changes across the system were measured by type T thermocouples (TC) placed at different depths. Temperature change history data was measured and recorded by an Agilent 34980A Multifunction data logger for comparison with a computer numerical model information representing the test. Ultimately, a numerical model was used for the calculation of the overall R-value of the system.

4.1 THE HFT COMPOSITE WALL SYSTEM

As shown in Figure 1, an HFT composite wall system (300mm×400mm×93mm) was sourced from a full-scale HFT wall system (500mm × 2000mm) presented in Fernando, et al. [12]. As it can be seen in the figure, the structural arrangement created a pattern of an air cavity formed by a hat section (the hat section air cavity)

https://doi.org/10.52202/080513-0099

followed by another air cavity created between hat sections (in-between air cavities).

To reduce the air movement during the heating process and recreate better the air cavities conditions closer to those potentially in a building, all edges of the sample were sealed by using 17mm timber plywood boards and steel screws.

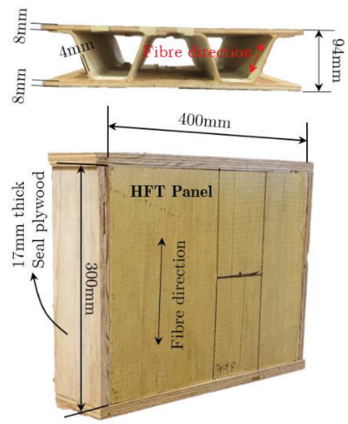

Figure 1 Configuration of the testing sample

4.2 THE SMALL-SCALE THERMAL TEST (SSTT)

The test set-up was illustrated in Figure 2a and Figure 2b. The calibrated heating lamp was employed as the heating source. The horizontal midplane of the heating lamp is aligned with the midplane of the sample. While the vertical centre line of the heating lamp was aligned with the middle line between Section A and B. Three distances between the heating lamp and the sample were used, they are 825mm, 925mm and 1025mm. To reduce the heat transfer between the HFT wall system and the steel base of the adjustable trolley, the HFT wall system sit on a 100mm thick insulation mat to create a simple thermal boundary for the sample. Then, the front side of the HFT wall system was adjusted to be parallel to the front plane of the heating lamp Figure 2a. The centre of Section B (highlighted by the red circle in Figure 2a was aligned with the centre of the heating lamp. Considering there might be damage caused by the heating in a closer distance, the temperature distribution along the thickness direction of the wall system was firstly measured at 1025mm away from the heating source plane. Then same test was then carried out at 925mm and 825mm distance Figure 2a. For each distance, the sample was heated up three times in separate days to obtain a reliable temperature distribution along the wall system thickness direction.

4.2.1 Quantification of the SSTT HFT wall system heat load conditions

Before carrying out the heating test, the heat flux of the lamp at different distances were measured. Due to the symmetry of the heat flux distribution, only a quarter of the area was mapped. While measuring the heat flux, the heat flux sensor was fixed at one position until the reading reaches a stable value. Then the sensor was moved to the next position. Such procedure was repeated

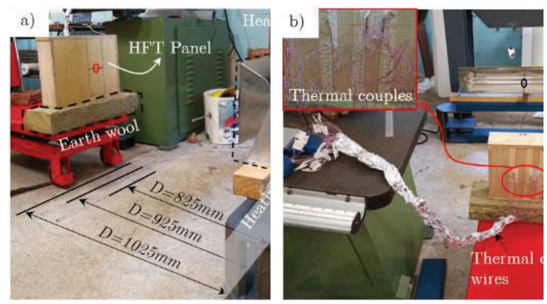

Figure 2 a) The front view of the test set-up; b) Back view of the test set-up

until enough data points were obtained for one measuring distance. Same steps were followed in the other distances. The measuring positions are illustrated in Figure 3 and the corresponding heat flux values at that point are presented in Figure 4. As the position further away from the centre of the heating source, the heat flux decreases significantly. The heat flux distribution shows an elliptical shape. Such heat flux distribution will be used as input in the numerical simulation.

4.3 THE NUMERICAL MODEL

Together with the SSTT, a numerical model using ANSYS Workbench R19.2 was developed. It represented a three-dimensional geometry of the HFT wall system, defined using AutoCAD, to calculate the temperature-histories at those points where the TC were located through the HFT composite wall system.

Following an inverse method, the temperature distribution measured was compared with those calculated, so that in the end the matching numerical parameters were determined, these are the heat loss coefficients associated to the heat load conditions and the apparent thermal properties of each wall system component.

https://doi.org/10.52202/080513-0099

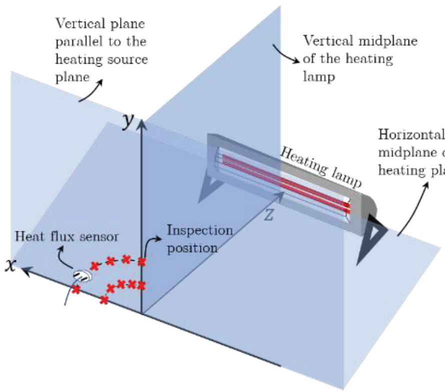

Figure 3 Schematic figure of the heat flux mapping and 825mm from the heating lamp

Once the model was validated, it was ready to obtain information that could be accurately used for design purposes. More detailed information about the numerical model can be found in previous studies [9].

This study focussed on calculating the overall R-value of the HFT system. To that end, the geometry representing the plywood of the HFT sample tested that closed the air gaps were removed, so that a more representative R-value of the real system used in buildings can be obtained. An arbitrary heat load condition was chosen and the boundary conditions of the edges of the system geometry considered adiabatic, so that the neat heat flow could be determined. Matching materials of the system obtained were used along with the matching heat transfer coefficients at both the exposed and non-exposed surfaces.

$$R_{c;op} = \frac{T_{exposed\,surface} - T_{non-exposed\,surface}}{q_{net}} \tag{1}$$

$$R_{value} = R_{c;op} + R_{si} + R_{se} \tag{2}$$

$$R_s = \frac{1}{h_T} \tag{3}$$

The numerical results came in the form of nodal data describing surface temperatures at both exposed and non-exposed surfaces, and the net neat flowing through the

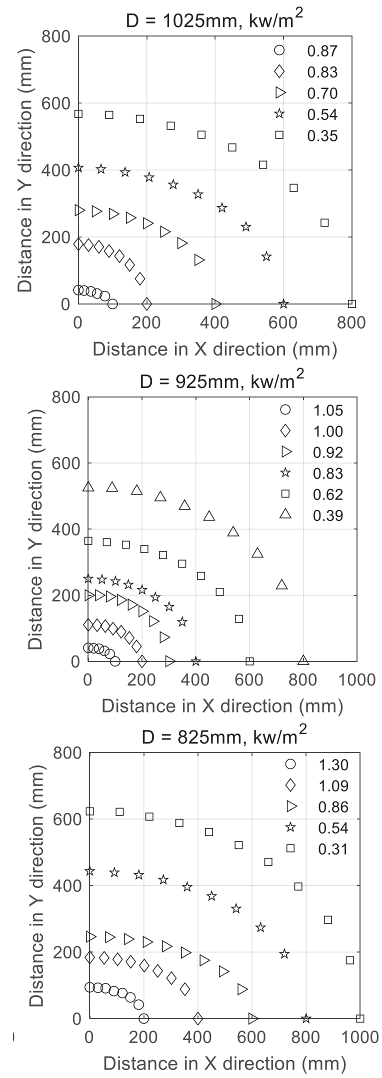

Figure 4 The heat flux mapping measured from 1025mm, 925mm

system. These information enables the calculation of the standardized surface-to-surface resistance Rc;op according to Eq. (1), which depends on the thermal properties of the materials of the system only [14]. As seen in Eq. (2), adding surface resistances would ultimately allow obtaining the pursued R-values. This study considered the surface resistance R_s according to Eq. (3).

4.3.1 Quantification of the influence of the thermal bridge

The influence of the thermal bridging elements on the HFT overall R-value is quantified by comparing the R-value of a hypothetical HFT system with no thermal bridges using the numerical model validated with the SSTT. To achieve such approach, the material properties associated to the geometry of the elements forming the thermal bridge need to match the adjacent material.

4.4 ANALYTICAL CALCULATION METHOD OF THE HFT WALL SYSTEM OVERALL R-VALUE

Building designers usually follow standardized analytical methods to estimate the R-values of building envelope components. As a reference, this study used the analytical method followed by CIBSE [15], so that it can be compared the result of this study and evaluated the differences.

5 RESULTS

Temperature along the wall system cross direction was measured using TC. shown in Figure 5, three sections (Section A, B and C) were selected to position three series of TCs. Section A and B were the midplane of one of the hat section air cavities and the midplane of the air cavity in-between respectively.

A preliminary analysis following the CIBSE analytical method suggested that the hat structural sections would act as thermal bridges and therefore would be detrimental for the overall R-value of the HFT system. To evaluate such approach in detail, Section C was considered as a third series of TCs located next to section B, both in the air cavity in-between hat sections, through the middle plane of the upper flange bonding with the face sheet..

For the face sheets on the Sections A to C, three TCs were positioned so that the temperature on the surface, inside and bi-layer interface could be measured. While for the flange of the hat section layer, only two TCs were fixed close to the edge of that layer due the difficulty in fixing the TCs in such thin layers. For the air cavities, three TCs were deployed close to the air-timber interface and in the middle of the air cavities section.

TCs at the surface of the wall system were fixed using insulation tape. While for TCs inside of the wall system, small holes (2mm in diameter) were drilled from the back of the wall system to the predetermined location. Then, TCs were attached to timber sticks and inserted to the desired locations (Figure 5 and Table 1). TCs were symmetrically arranged within 20mm height region to reduce the effect caused by the different heat flux. The depth of the drilling holes were carefully controlled for the subsequent temperature comparison with numerical simulation.

Only one HFT wall system was available for testing, so the SSTT was conducted applying heat flux to one side of the wall system only.

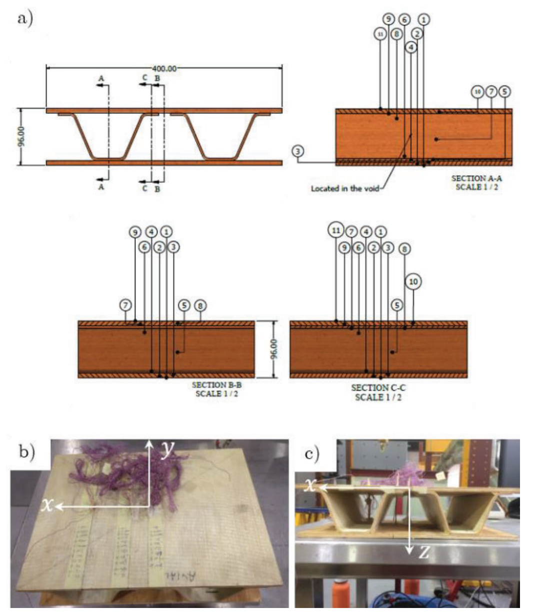

Figure 5 a) Schematic figure of the TC arrangement; b) The front view of the TCs; c) The section view of the TCs.

Table 1 Distance of the TC (TC) to the wall system front

Section A		Section B		Section C	
TC	Depth (mm)	TC	Depth (mm)	TC	Depth (mm)
A1	0	B1	0	C1	0
A2	2	B2	2	C2	2
A3	6	B3	6	C3	7
A4	9	B4	15	C4	15
A5	11	B5	45	C5	45
A6	15	B6	75	C6	75
A7	45	B7	87	C7	83
A8	75	B8	90	C8	85
A9	82	B9	93	C9	87
A10	90			C10	90
A11	93			C11	93

5.1 SSTT DATA MEASURED

A typical temperature profile in one test is presented in Figure 6. Since the TC A1 is on the surface of the wall system, thus a complicated thermal boundary was

 https://doi.org/10.52202/080513-0099

imposed, the reading of the TC showed a significant fluctuation. However, it generally showed the trend of the temperature change. The temperature at different positions were recorded before the heating lamp was switched on. Therefore, the temperature of the wall system is identical to that of the room temperature. As heating starts, the temperature at all positions first increased rapidly till around 25 minutes from heating start. Then, the temperature increased slowly till the end of the heating. Except TCs A9 to A11, the temperature dropped as the depth of the measurement point increases, i.e., from the heating front to the back of the wall system. After 6 hours of heating, the lamp was switched off and then the temperature dropped significantly and in the last reached the room temperature.

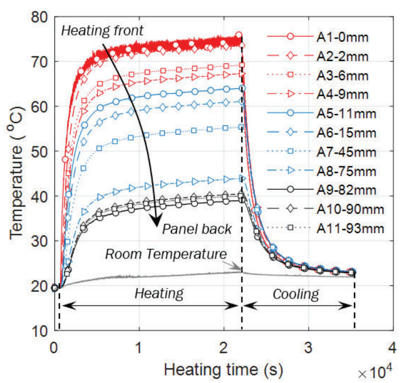

Figure 6 The temperature change during one test

The temperature distribution along the thickness direction of the wall system in different test scenarios is presented in Figure 7.

The following observations can be made:

1. Temperature distribution shows a very different pattern in different layers. In all measured sections, the temperature within the fibre laminated timber layer shows a higher temperature gradient than that in the hollow region.
2. The temperature distributions along Section-B and Section-C are almost the same since two sections are only 22mm away. The temperature along Section-A is slightly smaller than that at Section-B and C. The reason for such difference could be that more heat was transferred to the hat section bonded to the face sheet.
3. The temperature at the back of the wall system is about half of the temperature at the front of the wall system in the present testing.

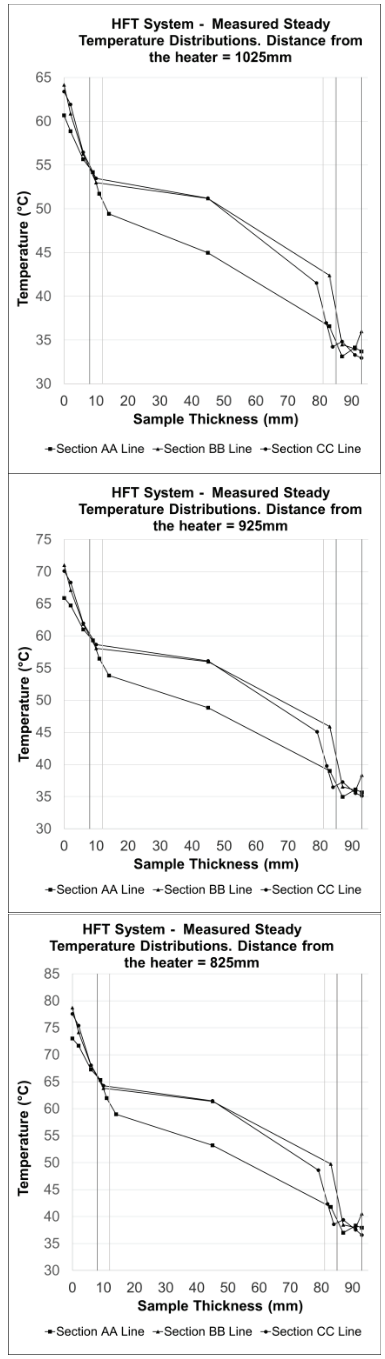

Figure 7 Temperature distribution measured at sections A to C when heating at test distances. Vertical lines represent the HFT system layers.

4. The temperature distribution in three separate tests for each tested distance shows very consistent results in terms of the temperature distribution shape and the temperature values. As wall system moves away from the heating lamp (from 825mm to 1025mm), the temperature decreases.
5. No standard error bars were included because tests were performed on one test sample only.

5.2 FEM FITTING PARAMETERS: COMPARISON OF MEASURED AND CALCULATED TEMPERATURE DISTRIBUTIONS

The geometry considered to model the HFT system included few simplifications that were carefully considered. On one hand, the GFRP laminated timber plywood of the sample tested was considered in the model as one volume only with one material associated because the layer of the GFRP was much thinner than the plywood, and furthermore, their material properties do not differ significantly. The volume of such wall systems was occupied mostly by plywood, so the inverse method started considering material properties of plywood available on the literature. While plywood generally would include orthotropic properties, this study considered it as an isotropic material. The apparent thermal conductivities associated to the HFT system materials shown in Table 2 were obtained following an inverse method comparing numerical temperature distributions through the model with the data measured from one test, and then validated with the other two tests. Acceptable values were considered when the deviation in all cases where below 10%.

Table 2 FEM fitting thermal conductivities input values

HFT Material	Thermal Conductivity (W/mK)
Plywood + GFR	0.12
Air	0.95

The numerical model boundary conditions were obtained following the same approach and criteria. The variation of the total heat losses h_t associated with the variation of the heat load applied to the HFT system is driven mainly by heat radiation losses. In this sense, the numerical model used included constant convection heat transfer coefficient h_c values at the surfaces of the system. The resulting matching values from the inverse process is shown in Table 3.

Table 3 Matching convective heat transfer hc obtained for the HFT wall system

System Surface	h_c (W/m²K)
Exposed	12
Not exposed	4

With the matching h_c values obtained, radiant heat transfer coefficient h_r values can be calculated for both the SSTT at surface points with temperature measured at sections AA, BB and CC and the associated calculated values. Table 4 shows the h_r values calculated together with the maximum difference between the h_r calculated from data measured and data calculated where it can be seen that deviations found between the two were lower than 3%.

Table 4 Mean Radiant heat transfer coefficients hr (W/m²K) calculated for the exposed surface of the HFT wall system

Wall system Surface	Method	D825 mm	D925mm	D1025mm
Exposed	SSTT	6.1	5.9	5.7
	FEM	6.3	5.9	5.7
	Max. deviation	2.45%	0.77%	0.02%
Non exposed	SSTT	5.1	5.0	4.9
	FEM	5.1	5.0	4.9
	Max. deviation	0.10%	-0.40%	-0.34%

Once the values of both h_c ad h_r are obtained, it can be estimated the total mean heat transfer coefficients for the system, which for the case of the HFT wall system are shown in Table 5, from where a correlation can be defined to estimate heat losses at different heat loads reaching the system as represented in Figure 8. Finally, matching temperature distributions calculated are represented together with the temperature distributions measured in Figure 9.

Table 5 Mean total heat transfer coefficients h_t (W/m²K) calculated for the HFT wall system

System Surface	D825mm	D925mm	D1075mm
Exposed	18.3	17.9	17.7
Not exposed	9.1	9.0	8.9

5.3 HFT OVERALL R-VALUE CALCULATION

The R-value of the HFT wall system were calculated by means of the numerical model validated with the SSTT and also by means of the CIBSE analytical method that was included as a design reference.

For the purposes of the R-value calculation, the test heat load conditions at a separation distance of 825mm from the radiant heater were used, therefore the resulting mean surface resistances values associated to this separation distance were used.

https://doi.org/10.52202/080513-0099

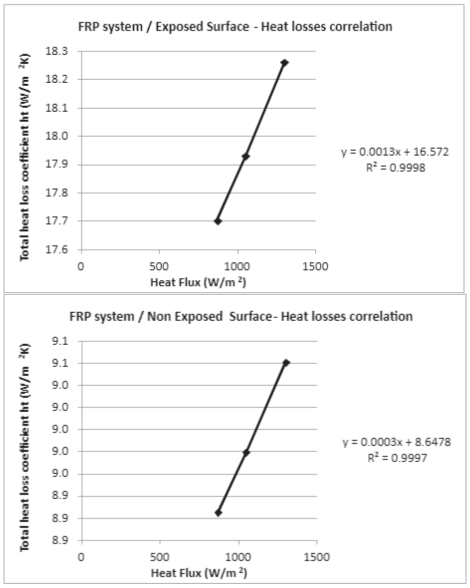

Figure 8 *Total heat losses correlation for the HFT system.*

Table 6 presents the mean surface resistances calculated using the values of the mean total heat transfer coefficients of Table 5 and Eq. (3), together with the standardized surface resistance that can be found in CIBSE Guide A [15].

Table 6 Mean surface resistance values (m²K/W) calculated for the HFT wall system

Rs	D 825mm	CIBSE
Rse	0.05	0.04
Rsi	0.11	0.13

The R-value calculated for the HFR system is presented in Table 8 where it can be seen the R-value calculated following the CIBSE analytical method and the R-value obtained following the method used along this study.

The CIBSE analytical calculations included the thermal conductivity of the plywood obtained from the inverse method followed by this study, however it followed the CIBSE method to estimate the thermal resistance of air spaces. Table 7 shows such a value together with the air resistance obtained by means of the method followed by this study, which appears to be about 64% lower than the value calculated through CIBSE method.

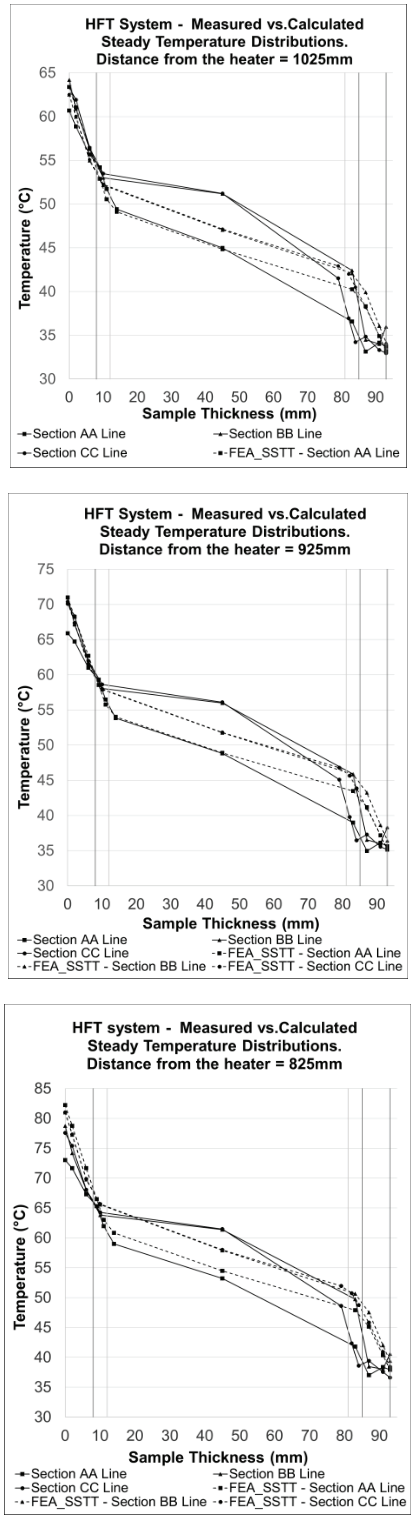

Figure 9 Temperature distribution within the HFT system: Measured vs calculated. Vertical lines represent the bounds of the different layers of the HFT system.

Table 7 Air cavity resistance. CIBSE vs TDA method

Method used	Ra (m²K/W)
CIBSE	0.23
TDA method	0.08

To evaluate the effect of the thermal bridges on the overall R-value, it was compared in both cases the R-value calculated with and without the structural elements acting as thermal bridges so that its effect can be evaluated, where the CIBSE analytical method uses the Combined method to account for the effect of the thermal bridges.

Table 8 Estimated R-vlaue for the HFR system.

Method applied	Thermal Bridge	R-value ((m²K/W)
Analytical	No	0.53
	Yes	0.34
Numerical	No	0.38
	Yes	0.40

6 DISCUSSION

The air cavity thermal resistance measured for the HFT wall system resulted significantly lower than the one calculated by means of the CIBSE analytical method. If the effect of thermal bridges is not considered for design purposes, the consequence of this deviation would be that the thermal insulating properties under steady heat conditions of the HFT wall system would be overestimated if only the CIBSE analytical method is considered. Hence, the deviation on the estimated energy needed to keep comfort conditions in a building would be underestimated and more energy would be consumed.

Generally, standardised Analytical methods follow the same approach [14] [16], therefore the same deviation would have been encountered. Furthermore, standards defining the equivalent thermal conductivity of air cavities that have to be used as input data in numerical calculations refers to the values calculated by means the standardised analytical methods [17], therefore, the design of the HFT system under study would have been influenced by such deviation if only the standard value would have been considered.

On the other hand, the CIBSE analytical results show that the effect of the thermal bridges on the overall R-value are caused by the structural elements of the system being important and visibly detrimental, reducing the insulation properties of the HFT system over 36%. Such approach is generally accepted by the design community.

Surprisingly, however, this study demonstrated that for the HFT system under study, a thermal bridge effect is not caused by the structural elements. The overall R-value appears to be improved when the structural elements are deemed into consideration by 5%. The beneficial effect however is not relevant because the thermal conductivity of the plywood did not defer much from that of the air cavity.

For the system of this study in particular the information obtained enhanced the design decision making process of the HFT system by clarifying, for example, that the overall R-value might be improved by filling the air cavities with an insulating material that prevent the internal movement of the air.

7 CONCLUSION

This study demonstrated that there can be building envelope designs where unventilated air cavities can conduct more heat than the structural elements.

Such conclusion can only be demonstrated by using methods to quantify R-values capable to describe the internal heat flow process of building components, such as the TDA method.

Higher design stages require higher characterisation refinement. Thus, the number of tests needed depend on the level of detail and verification required by the design stage of the design process.

The surface resistances calculated from the SSTT did not differ much from those suggested by CIBSE.

This study found discrepancies between the R-value of the air cavity calculated by means of the method followed by this study and the values calculated by either analytical or numerical standardized methods. In this sense, this study suggests conducting further work to understand better such discrepancies.

8 ACKNOWLEDGEMENTS

The authors appreciate the invaluable effort done by The Centre for Future Timber Structures, the UQ Fire Group, EPORA Engineering Pty Ltd and the partners involved in this study to achieve all the research objectives.

9 REFERENCES

[1] "IEA (2022), World Energy Outlook 2022, IEA, Paris https://www.iea.org/reports/world-energy-outlook-2022, License: CC BY 4.0 (report); CC BY NC SA 4.0 (Annex A)," ed.

[2] M. G. Davies, *Building heat transfer*. John Wiley & Sons, 2004.

[3] *C1363-19: Standard Test Method for Thermal Performance of Building Materials and Envelope Assemblies by Means of a Hot Box Apparatus*, 2019.

[4] "BS EN ISO 8990-1996: Thermal insulation — Determination of steady-state thermal

https://doi.org/10.52202/080513-0099

transmission properties — Calibrated and guarded hot box," ed: British Standards Institute.

[5] R. American Society of Heating and I. Air-Conditioning Engineers, *2021 ASHRAE® Handbook - Fundamentals (SI Edition)*. American Society of Heating, Refrigerating and Air-Conditioning Engineers, Inc. (ASHRAE), 2021.

[6] B. Peters, A. Sharag-Eldin, and B. Callaghan, "Development of a simple Hot Box to determine the thermal characteristics of a three-dimensional printed bricks," in *Proceedings of the ARCC 2017 Conference—Architecture of Complexity, Salt Lake City, UT, USA*, 2017, pp. 14-17.

[7] K. Trgala, M. Pavelek, and R. Wimmer, "Energy performance of five different building envelope structures using a modified Guarded Hot Box apparatus—Comparative analysis," *Energy and buildings,* vol. 195, pp. 116-125, 2019.

[8] A. Stonkuvienė, A. Burlingis, J. Ramanauskas, and K. Banionis, "Determination of core thermal resistance errors of reflective multifoil insulation products measured in a hot box depending on evaluation accuracy of its low emissivity surfaces," *Journal of Building Engineering,* vol. 59, p. 105143, 2022/11/01/ 2022.

[9] G. Soret, D. Lázaro, J. Carrascal, D. Alvear, M. Aitchison, and J. Torero, "Thermal characterization of building assemblies by means of transient data assimilation," *Energy and Buildings,* vol. 155, pp. 128-142, 2017.

[10] K. Boswell, *Exterior building enclosures: design process and composition for innovative façades*. John Wiley & Sons, 2013.

[11] S. J. Chang, S. Wi, and S. Kim, "Thermal bridging analysis of connections in cross-laminated timber buildings based on ISO 10211," *Construction & building materials,* vol. 213, pp. 709-722, 2019.

[12] D. Fernando, J. G. Teng, J. Gattas, and M. Heitzmann, "Hybrid fibre-reinforced polymer–timber thin-walled structural members," *Advances in Structural Engineering,* vol. 21, no. 9, pp. 1409-1417, 2017.

[13] D. Fernando, J. Teng, J. Gattas, and M. Heitzmann, "Hybrid fibre-reinforced polymer–timber thin-walled structural members," *Advances in Structural Engineering,* vol. 21, no. 9, pp. 1409-1417, 2018.

[14] "BS EN ISO 6946:2017: Building components and building elements. Thermal resistance and thermal transmittance. Calculation methods," ed: British Standards Institute, 2022.

[15] Cibse, "3.3 Heat Losses from Buildings," in *Environmental Design - CIBSE Guide A (8th Edition)*: The Chartered Institution of Building Services Engineers (CIBSE).

[16] "AS/NZS 4859.2:2018: Thermal insulation materials for buildings," ed: SAI Global Australia Pty Ltd.

[17] "BS EN ISO 10211:2017: Thermal bridges in building construction - Heat flows and surface temperatures - Detailed calculations," ed: British Standards Institute.